Original Article



DysUFMylation of SREBP1 Promotes the Progression of Hepatocellular Carcinoma by Reprogramming Lipid Metabolism



Xukang Gao^{1,2,3#}, Zeping Han^{1,2,3#}, Min Xu⁴, Zhutao Wang^{1,2,3}, Guoqiang Sun^{1,2,3}, Hao Xiao^{1,2,3}, Dai Zhang¹, Shuangjian Qiu^{1,2,3}, Ning Ren^{1,2,3}, Chenhao Zhou^{1,2,3*} and Yong Yi^{1,2,3*}

¹Department of Liver Surgery and Transplantation, Zhongshan Hospital, Fudan University, Shanghai, China; ²Liver Cancer Institute, Zhongshan Hospital, Fudan University, Shanghai, China; ³Key Laboratory of Carcinogenesis and Cancer Invasion, Fudan University, Ministry of Education, Shanghai, China; ⁴Department of Thoracic Surgery, Shanghai Tenth People's Hospital, School of Medicine, Tongji University, Shanghai, China

Received: June 30, 2025 | Revised: August 27, 2025 | Accepted: September 23, 2025 | Published online: October 22, 2025

Abstract

Background and Aims: Sterol regulatory element-binding protein 1 (SREBP1), a key regulator of lipogenesis, is highly expressed in tumors, but the mechanisms sustaining its elevated levels remain unclear. The role of UFMylation, a posttranslational modification, in modulating SREBP1 stability and tumor progression has not been explored. This study aimed to investigate the role of UFMylation in the progression of liver cancer. Methods: Liquid chromatography-tandem mass spectrometry was employed to investigate the interacting proteins of ubiquitin-fold modifier 1-specific ligase 1 (UFL1). Knockdown of UFL1 and DDRGK domain-containing protein 1 (DDRGK1) was performed to assess SREBP1 stability. In vitro and in vivo models of hepatocellular carcinoma (HCC) were used to evaluate tumor progression. Clinical correlations between UFL1/DDRGK1 and SREBP1 levels were analyzed in HCC patient samples. Results: SREBP1 undergoes UFMylation, which synergizes with ubiquitination to reduce its stability. Depletion of UFL1 or DDRGK1 increased SREBP1 stability, driving HCC progression. Clinically, UFL1 and DDRGK1 levels were reduced in HCC tissues and inversely correlated with SREBP1 expression. Fatostatin (an SREBP1 inhibitor) enhanced the therapeutic effect of Lenvatinib in HCC models with low UFL1 expression. Conclusions: UFMylation is a critical posttranslational modification that destabilizes SREBP1, and its dysregulation contributes to HCC progression. Targeting the UFMylation-SREBP1 axis, particularly through Fatostatin and Lenvatinib combination therapy, represents a novel therapeutic strategy for HCC.

Citation of this article: Gao X, Han Z, Xu M, Wang Z, Sun G, Xiao H, et al. DysUFMylation of SREBP1 Promotes the Pro-

Keywords: Hepatocellular carcinoma; HCC; ubiquitin-fold modifier 1-specific ligase 1-specific ligase 1; UFL1; UFMylation; Sterol regulatory element-binding protein 1; SREBP1.

gression of Hepatocellular Carcinoma by Reprogramming Lipid Metabolism. J Clin Transl Hepatol 2025;13(11):949-963. doi: 10.14218/JCTH.2025.00318.

Introduction

Hepatocellular carcinoma (HCC) is the most prevalent liver cancer globally, ranking as the sixth most common cancer and the third deadliest. Some patients with early-stage HCC can receive curative treatments, including liver resection, liver transplantation, and radiofrequency ablation, among others. However, most patients are diagnosed with advanced HCC, resulting in a five-year survival rate of approximately 12%. This low rate is largely due to limited treatment options and the poor effectiveness of first-line therapies.²

UFMylation is a ubiquitin-like posttranslational modification in which ubiquitin-fold modifier 1 (UFM1) is conjugated to target proteins. Since its initial discovery in 2004, UFMylation has been found to be closely associated with a wide range of diseases, including diabetes, ischemic heart disease, heart failure, hematologic disorders, atherosclerosis, and tumors.3 Like other modifications, UFMylation requires a three-step enzyme system consisting of E1, E2, and E3 enzymes.4 However, to date, only one E1 enzyme: ubiquitin like modifier activating enzyme 5 (UBA5), one E2 enzyme: ubiquitin-fold modifier conjugating enzyme 1 (UFC1), and one E3 enzyme (UFL1) have been identified in the UFMylation system. Mature UFM1 is activated by UBA5 in an ATP-dependent manner and then transferred to UFC1. Finally, UFM1 is covalently conjugated to target proteins via UFL1.5 DDRGK1 (UFBP1), the first identified target of the UFM1 system, plays an essential role as a substrate for UFL1 as well as in the UFMylation of other proteins. 6-9 In addition, DDRGK1 can enhance the anchoring of UFL1 to the endoplasmic reticulum, thereby facilitating its function. 10 Several studies have demonstrated that the UFM1 system plays a critical role in maintaining endoplasmic reticulum homeostasis and in embryonic development.11-15 Emerging evidence extends the functional scope of UFMylation to fatty acid metabolism, with recent studies

^{*}Contributed to this work equally.

^{*}Correspondence to: Yong Yi and Chenhao Zhou, Department of Liver Surgery and Transplantation, Liver Cancer Institute, Zhongshan Hospital, Fudan University, 180 Fenglin Road, Shanghai 200032, China. ORCID: https://orcid.org/0000-0002-4800-3249 (CZ). Tel/Fax: +86-21-64041990, E-mail: yi.yong@ zs-hospital.sh.cn (YY) and zhouchenhao@fudan.edu.cn (CZ).

demonstrating that DDRGK1 UFMylation exerts suppressive effects on hepatic lipogenesis.³ Recently, an increasing number of UFMylation substrates, including programmed cell death protein 1, programmed cell death 1 ligand 1, and tumor protein 53, have been identified.^{6,7,9} To date, the biological significance of the UFM1 system, particularly in tumor development, remains poorly understood.

Metabolic abnormalities are key characteristics of tumor development. To acquire more nutrients, tumors often generate an abundance of blood vessels and compete with surrounding cells for these essential resources. The metabolic pathways that change mainly include glucose, amino acid, and lipid metabolism. ¹⁶⁻¹⁸ In recent years, increasing attention has been given to the role of metabolism, particularly lipid metabolism, in tumor development. ^{19,20} The liver plays a crucial role in lipid metabolism, and abnormalities in lipid metabolism are often present throughout the entire process of HCC development. ²¹ However, the effects of UFMylation on tumor metabolism are not yet fully understood.

Enhanced lipid metabolism is one of the most significant characteristics of cancer. ²² SREBP1, a well-known master regulator of lipogenesis, plays a crucial role in the progression of various tumors. ^{23–25} SREBP1 is synthesized and resides in the endoplasmic reticulum as an inactive precursor. When sterol levels are deficient, the SREBP1 precursor undergoes two proteolytic cleavages, allowing it to enter the nucleus as the mature protein. This active form promotes the transcription of target genes, thereby activating lipid synthesis and uptake. Interestingly, tumors often exhibit high expression levels of SREBP1, leading to enhanced lipid metabolism.

Here, we report that SREBP1 is a substrate of UFMylation. Reduced expression of UFL1 or DDRGK1 decreases the UFMylation of SREBP1, which enhances its stability by counteracting its ubiquitination. This process activates lipid synthesis and promotes the progression of HCC. Furthermore, SREBP1 may serve as a potential therapeutic target for HCC patients with low UFMylation levels.

Methods

Patients and specimens

For the construction of the tissue microarray, 98 tumor tissues and adjacent nontumor tissues certified by pathologists were obtained from patients with HCC who underwent treatment at Zhongshan Hospital between January 1, 2009, and January 1, 2010 (cohort 1). The inclusion criteria and followup procedures were performed as previously described.²⁶ The clinicopathologic characteristics of these patients are summarized in Supplementary Tables 1 and 2. We randomly selected 30 paired frozen samples from cohort 1 to detect messenger RNA (mRNA) expression of UFL1 and DDRGK1, and 30 paired samples to detect protein expression of UFL1, DDRGK1, and SREBP1. Overall survival was calculated as the time interval between the date of hepatectomy and death or last follow-up. Recurrence-free survival was determined from the date of hepatectomy to tumor recurrence or last follow-up.²⁷ The prognosis of HCC patients in tissue microarray (TMA) is summarized in Supplementary Table 3. The study protocol was thoroughly reviewed and approved by the Research Ethics Committee of Zhongshan Hospital, Fudan University, and adhered strictly to the ethical principles outlined in the Declaration of Helsinki. All patients provided written informed consent prior to therapy and inclusion in the study.

Cell lines and cell culture

HEK293T cells and HCC cell lines MHCC97H, SNU-449, PLC/

PRF/5, HCCLM3, Huh7, and HepG2 were obtained from the Liver Cancer Institute, Fudan University, Shanghai, China. The Hep3B cell line was purchased from the Cell Bank of the Chinese Academy of Sciences (Shanghai, China). All of these cells were cultured in high-glucose Dulbecco's modified Eagle's medium (DMEM) supplemented with 10% fetal bovine serum (FBS) and 1% penicillin and 100 μg/mL streptomycin in a humidified incubator containing 5% CO2 at 37°C.²⁸

Plasmids and establishment of stable cell lines

The short hairpin RNAs (shRNAs) targeting UFL1 and DDRGK1 were inserted into the LV3 (H1/GFP-Puro) plasmid by GenePharma (Shanghai, China). The shRNAs targeting SREBP1 were inserted into the LV3 (H1/GFP-Hyg) plasmid by GenePharma (Shanghai, China). HA-UFC1, HA-UBA5, HA-UFL1, MYC-DDRGK1, and Flag-SREBP1c plasmids were purchased from Youbio Company (Hunan, China). To construct stable cell lines with downregulation of UFL1, DDRGK1, and SREBP1, lentiviral vectors were constructed based on the above plasmids and transfected accordingly. The plasmid was transfected into cells and selected with 2 μ g/mL puromycin or puromycin (2 μ g/mL) + hygromycin B (50 μ g/mL).²⁹ The sequences of the shRNAs used were as follows:

- UFL1-1, 5'-CCAGTAAGCATAAGTCATATT-3'
- UFL1-2, 5'-GTGGTCGAGTAAACATTGT-3'
- UFL1-3, 5'-GCAGCCATTACAAGTGATA-3'
- DDRGK1-1, 5'- GGCTCTGCTAGTCGGCTTTAT-3'
- DDRGK1-2, 5'- GCCTACGCACTCAGGACACCA-3'
- DDRGK1-3, 5'- GGACTATAACAGGTGTGATTG-3'
- SREBP1, 5'-GCUCUGCGAGUGGAUGCUATT-3'

Antibodies and reagents

The following antibodies were used in the present study: anti-UFL1 (Proteintech, 26087-1-AP, China), anti-DDRGK1 (Proteintech, 21445-1-AP), anti-UFM1 (Proteintech, 15883-1-AP), anti-SREBP1 (HUABIO, HA500210 and HA722160, China), anti- β -ACTIN (Abmart, P60035S, China), anti-ubiquitin (Abmart, T55965), anti-HA (Beyotime, AF2861, China), anti-MYC (Beyotime, AF2867), and anti-Flag (Beyotime, AF2855). The following reagents were used in the experiments: Fatostatin (HY-14452), Cycloheximide (CHX; HY-12320), MG-132 (HY-13259), Chloroquine (HY-17589A), and Lenvatinib (HY-10981), all purchased from MedChemExpress (USA).

Western blot analysis and immunoprecipitation

Proteins were extracted by lysing cultured cells in RIPA buffer containing protease inhibitors and quantified using a BCA assay kit. Heat-denatured proteins mixed with 5x loading buffer were separated by SDS-PAGE and then transferred onto PVDF or NC membranes (Millipore, USA). The membrane was blocked with 5% skim milk. Bands were exposed with enhanced chemiluminescence reagents using ImageQuant™ LAS 4000 after incubation with the indicated primary antibodies followed by HRP-conjugated secondary antibody. 30 Western blot analysis of target proteins was performed using ImageJ. Band intensities were quantified in ImageJ using the Gel Analyzer. For each lane, regions of interest were defined with identical dimensions, and local background was subtracted. Target protein signals were normalized to the corresponding loading control (β-ACTIN). Data were further referenced to the mean of the control group, which was set

For immunoprecipitation, cell lysates were incubated with the indicated antibodies at 4°C overnight on a vertical rotator and then rotated for 2 h at 4°C in the presence of protein A/G

beads. The beads were washed five times with lysis buffer and mixed with SDS-PAGE loading buffer for immunoblotting. $^{\rm 31}$

RNA isolation and quantitative real-time polymerase chain reaction (PCR)

Total mRNA was isolated with a total RNA isolation kit (BioTeke Corporation, Beijing, China) and reverse transcribed into cDNA using a HiScript Q RT SuperMix for quantitative PCR kit (Vazyme Biotech, Nanjing, China) according to the manufacturer's instructions. PCR amplification products were quantified with SYBR Green PCR Master Mix (Vazyme Biotech) following a standard procedure. The expression of the target gene was normalized to that of the housekeeping gene $\beta\text{-}ACTIN$ and quantified using the $\Delta\Delta$ Ct method. The sequences of the primers used for quantitative real-time PCR were shown in Supplementary Table 4.

Immunohistochemistry

After deparaffinization, rehydration, and antigen retrieval, slides were incubated with the indicated primary antibodies, followed by staining with an HRP-conjugated secondary antibody.³³ Then, slides were scanned and viewed in the KF-Viewer software. The staining results were assessed independently by two pathologists who were unaware of the patients' clinical characteristics, using the H-score method.³⁴

Colony formation and 5-bromo-2'-deoxyuridine (EdU) incorporation assays

For colony formation assays, cells were seeded in six-well plates (1 \times 10³ cells per well) and maintained in complete medium containing 10% FBS for 14 days. Colonies were fixed with 4% paraformaldehyde solution and stained with 0.1% crystal violet.³⁵

EdU incorporation assays were performed using an EdU kit (Beyotime, C0078) to validate the cell proliferation ability. Cells were plated in 24-well plates (1 \times 10⁵ cells per well), and the experimental procedures were conducted in accordance with the manufacturer's instructions.³⁶

Wound healing assays

HCC cells were seeded in six-well plates. When the cells formed a compact monolayer, a 200-µL tip was used to create a scratch. The wells were then washed three times with phosphate-buffered saline (PBS). Afterward, DMEM containing 1% FBS was added to each well.³⁷ The progression of wound closure was evaluated by imaging at specified intervals using an IX71 inverted microscope (Olympus Corporation, Japan). Finally, images were analyzed using ImageJ software

Transwell-migration and invasion assays

Transwell assays were performed to evaluate migration and invasion activities. For migration assays, 5×10^4 cells were seeded in the upper chamber with a non-coated membrane (24-well insert, pore size 8 μm ; Corning, USA) in DMEM containing 1% FBS. For invasion assays, 5×10^4 cells were seeded in the upper chamber with a Matrigel-coated (Beyotime, C037) membrane. In both assays, the lower chambers contained DMEM with 10% FBS as a chemoattractant. Cells were incubated at 37°C for 48 h. Cotton swabs were carefully used to remove the cells remaining in the upper chambers, while the cells that had migrated to the bottom surface of the membrane were fixed using 4% paraformaldehyde solution, stained with 0.1% crystal violet, and then counted under a

microscope.38

Multiplex immunofluorescence (mIF) assay

Cells were plated on glass coverslips and fixed with 4% paraformaldehyde for 15 m. After permeabilization using 0.5% Triton X-100 for 15 m, 5% BSA was used to block nonspecific binding sites. The cells were incubated with specific primary antibodies at 4°C overnight in a humidified box. After washing five times with TBST, the corresponding secondary horseradish peroxidase-conjugated antibody was used to incubate the cells. The coverslips were then washed with PBS in the dark and stained with 4',6-diamidino-2-phenylindole (Beyotime, C1005).³³ Images were captured using a laser confocal microscope (Olympus LV3000, Tokyo, Japan).

Oil Red staining

Cells were counted and plated into a six-well plate (1 \times 10⁵ cells per well). Twenty-four hours later, Oil Red O (Beyotime, C0158) staining was performed according to the manufacturer's instructions. Briefly, cells were gently aspirated to remove the culture medium and washed once with PBS, then fixed with 4% paraformaldehyde for 10 m at room temperature. After fixation, samples were rinsed twice with PBS. A staining rinse solution was added to cover the cells for 20 s, followed by its removal. Cells were subsequently incubated with freshly prepared Oil Red O working solution for 15 m at room temperature. After staining, the Oil Red O solution was discarded, and cells were briefly washed with the staining rinse solution for 30 s. Residual dye was removed by washing with PBS for 20 s. For nuclear counterstaining, cells were incubated with hematoxylin (Beyotime, C0107) for 8 m, followed by rinsing with distilled water to remove excess stain. Finally, PBS was added to cover the cells evenly.³⁹ Images were acquired using a light microscope.

Nile Red staining

Cells were counted and plated into a six-well plate (1×10^5 cells per well). Twenty-four hours later, Nile Red (Applygen Technologies Inc, C0009, China) staining was performed according to the manufacturer's instructions. Briefly, cells were gently aspirated to remove the culture medium and washed once with PBS, then fixed with 4% paraformaldehyde for 10 m at room temperature. Cells were incubated with Nile Red working solution for 10 m at room temperature. After staining, samples were rinsed once with distilled water. Fluorescence was observed immediately under a fluorescence microscope.

Triglyceride (TG), cholesterol (CHOL), and free fatty acid (FFA) measurement

Intracellular and intratumoral TG, CHOL, and FFA contents were assayed using kits purchased from Nanjing Jiancheng Bioengineering Institute and Applygen Technologies Inc.^{41–43} According to the manufacturer's recommended protocols. The values were normalized to cellular protein, and the protein concentration was determined using the BCA Protein Assay Kit (Beyotime, P0010).

Liquid chromatography-tandem mass spectrometry (LC-MS/MS) analysis

LC-MS/MS analysis was used to detect the potentially interacting proteins of the target protein. To identify the UFL1-interacting proteins, HA-UFL1 and vector controls were transfected into Huh-7 cells. Immunoprecipitates of UFL1 in Huh-7 cells were separated by SDS-PAGE and observed us-

ing Coomassie Blue staining. The gels were cut into slices and enzymatically digested according to a pre-stained protein marker. Next, LC-MS/MS was performed on an Orbitrap Elite mass spectrometer (Thermo Fisher Scientific) according to the manufacturer's instructions.⁴⁴ The peptides were then evaluated using a fragment spectra search against the Uni-Prot protein database (https://www.uniprot.org/) employing the Mascot search engine (version 2.3.0, Matrix Science).

In vivo tumor growth and metastasis assays

All procedures using four- to six-week-old male BALB/c nude mice were approved by the Institutional Animal Care and Use Committee of Zhongshan Hospital, Fudan University (2024-034). All mice were purchased from the Charles River Laboratory (Beijing, China) and housed in a temperature-controlled, specific-pathogen-free animal laboratory. For the establishment of subcutaneous xenograft models, 1×10^7 cells were injected into the right inguinal fold regions of BALB/c nude mice. Subsequently, tumors were resected and cut into 1 $\rm mm^3$ pieces. Sections of these subcutaneous tumors were orthotopically implanted into the livers of nude mice to establish orthotopic xenograft models. 45 Finally, the mice were euthanized four weeks after the experiments.

To establish pulmonary metastasis models, approximately 5×10^6 cells were injected into the tail vein of the mice. After four weeks, the mice were euthanized, and their lungs were excised and prepared for H&E staining. Microscopic counting was conducted to accurately determine the average number of metastatic foci in each group.

In vivo drug studies

One week after implantation, the mice were treated with Lenvatinib (30 mg/kg/day, intragastric administration) or Fatostatin (25 mg/kg, three times per week, intraperitoneal injection), ^{46,47} all purchased from MedChemExpress. After three weeks, the mice were sacrificed, and the tumors were collected for further study (photography, weighing, measuring).

Statistical analysis

Statistical analyses were conducted using SPSS version 27.0 software. Graphical representations were generated with GraphPad Prism 9 and R Studio 4.4.0 software. The chisquare test or Fisher's exact test was used to compare qualitative variables, and Student's t-test was used to compare continuous variables. Kaplan–Meier analysis was applied to assess survival, and the log-rank test was utilized to compare patient survival between subgroups. Multivariate analyses were conducted using a multivariate Cox proportional hazards regression model. The data are presented as means \pm standard deviations, and a difference was considered significant when the P- value was less than 0.05.

Results

Low expression of UFL1 or DDRGK1 is associated with poor prognosis in HCC patients

To clarify the role of UFMylation in HCC, we conducted TMA analysis and found that the expression levels of UFL1 and DDRGK1 in cancer tissues were lower than those in adjacent normal tissues (Fig. 1A and B), and low expression of UFL1 and DDRGK1 was associated with poor prognosis (Fig. 1C). In addition, the results of quantitative real-time PCR and Western blot analyses of HCC tissue and adjacent normal tissue also revealed that the expression of UFL1 and DDRGK1 in cancer tissue was lower than that in adjacent

normal tissue (Fig. 1D and E). We also measured UFMylation levels in tumor tissues and adjacent non-tumor tissues. The results demonstrated that UFMylation levels were significantly lower in tumor tissues compared to matched adjacent tissues (Fig. 1F). Therefore, UFMylation levels are reduced in HCC, and this decrease is associated with the prognosis of HCC patients.

Dysregulation of UFMylation in SREBP1 antagonizes its proteasome-mediated degradation

Here, we aimed to determine how UFL1 influences the development of HCC. Given that UFL1 is an E3 enzyme, we performed mass spectrometry to identify the proteins modified by UFL1. Notably, SREBP1, a well-known transcriptional regulator involved in lipid metabolism, was detected in the immunoprecipitates by mass spectrometry and received the highest scores (Fig. 2A-C). We then validated the mass spectrometry results in 293T cells, confirming that SREBP1, UFL1, and DDRGK1 can bind each other (Fig. 2D and Supplementary Fig. 1A). Our coimmunoprecipitation results in Huh-7 cells further revealed that SREBP1, UFL1, and DDRGK1 can bind each other (Fig. 2E and Supplementary Fig. 1B). Additionally, our multiplex immunofluorescence results demonstrated that SREBP1, UFL1, and DDRGK1 are co-expressed and have the potential to interact (Fig. 2F). These data suggest that SREBP1 may serve as a substrate for UFMylation.

To determine whether SREBP1 undergoes UFMylation, we co-expressed SREBP1 with UFMylation components, including UBA5, UFC1, UFL1, DDRGK1, and UFM1, in 293T cells. Previous studies revealed that the UFM1 precursor is an 85-amino acid protein. In humans, UFM1 specific peptidase 1/ UFM1 specific peptidase 2 cleaves off the two C-terminal residues (Ser84 and Cys85) to expose Gly83 as the new C-terminus, forming mature UFM1 (83 amino acids).⁴ Since Gly83 is essential for UFM1 functionality, we generated three mutants: ΔC2 (deletion of residues 84-85), ΔC3 (deletion of residues 83-85), and G83A (substitution of Gly83 with Ala). We found that SREBP1 can be UFMylated by wild-type UFM1 (UFM1WT) and UFM1 with an exposed carboxy (C)terminal glycine 83 residue (UFM1 $^{\Delta C2}$), but that UFMylation does not occur when UFM1 lacking the C-terminal glycine 83 residue (UFM1^{ΔC3}) or Gly83 of UFM1 is mutated to Ala (UFM- 1^{G83A}) (Fig. 2G).⁴ Moreover, we confirmed that UFMylation of SREBP1 can also occur in Huh-7 cells (Supplementary Fig. 1C). In summary, SREBP1 can bind to UFL1 and DDRGK1, leading to UFMylation.

To determine the effect of UFMylation on SREBP1, we first investigated the expression of UFL1 and DDRGK1 in HCC cell lines (Supplementary Fig. 1D). Next, we knocked down UFL1 and DDRGK1 in Huh-7 and HepG2 cells via shRNA. We found that knockdown of UFL1 or DDRGK1 significantly increased SREBP1 protein levels but did not affect SREBP1 messenger RNA levels (Fig. 2H and Supplementary Fig. 1E-G). Then, we examined the expression levels of SREBP1 in eight paired cancer tissues and adjacent normal tissues from patients with HCC (related to Fig. 1E). The results revealed that SREBP1 was more highly expressed in tumor tissue than in adjacent normal tissue (Supplementary Fig. 1H). These findings suggest that UFMylation may affect the protein stability of SREBP1. To further confirm this, we assessed the effect of UFMylation on SREBP1 stability in cells treated with cycloheximide and found that SREBP1 stability increased following the knockdown of UFL1 or DDRGK1 (Fig. 2I and Supplementary Fig. 1I). We subsequently inhibited the ubiquitin-proteasome pathway and the lysosomal pathway via MG132 and chloroquine, respectively. The results indicated that dysregulation of UFMylation may antagonize the proteasome-mediated

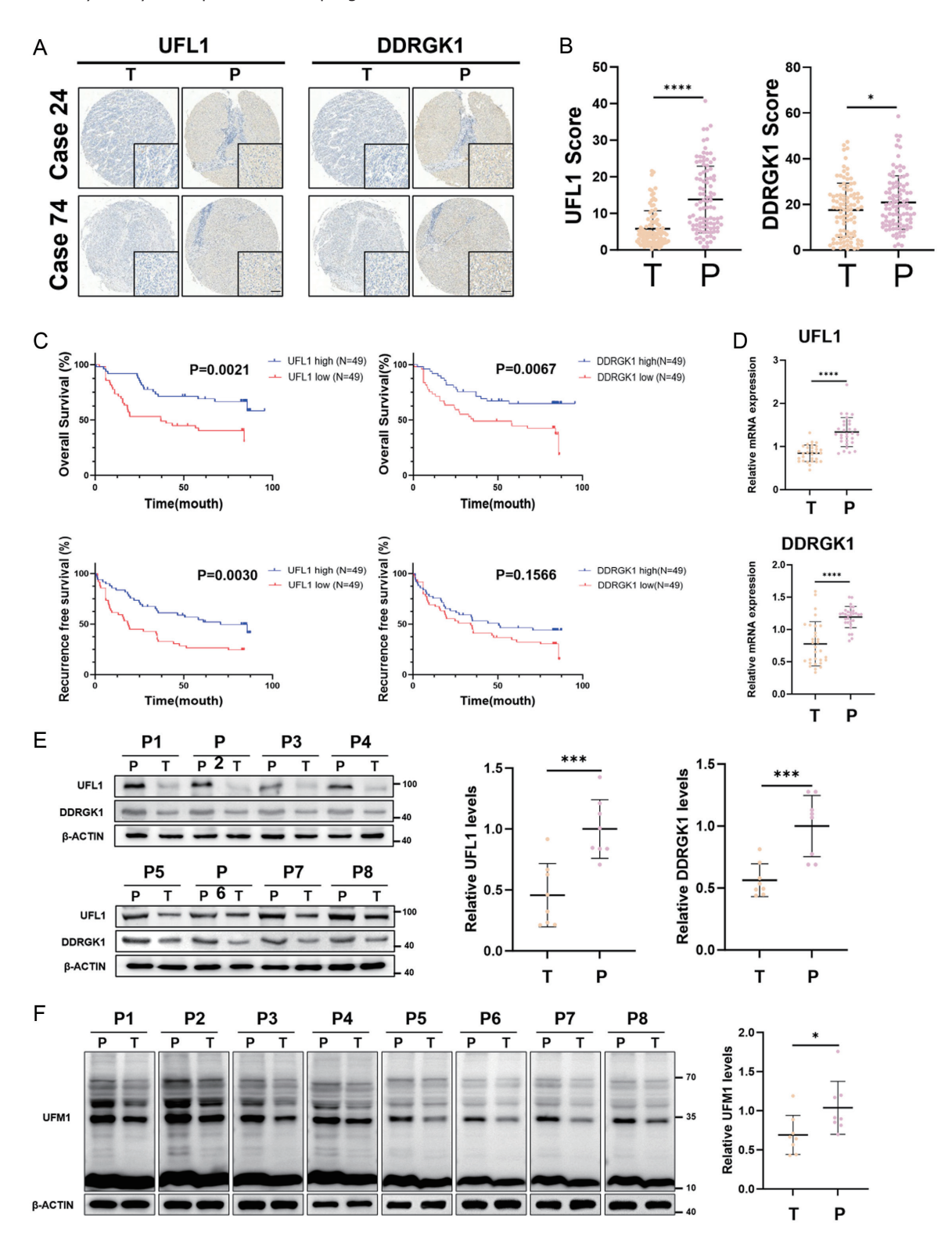


Fig. 1. UFL1 and DDRGK1 expression in HCC and their relationship with clinical outcomes. (A) Representative immunohistochemical staining for UFL1 and DDRGK1 in 98 pairs of HCC and adjacent normal tissues from tissue microarrays. Scale bars, $50 \mu m$ (left) and $5 \mu m$ (right). (B) Quantification of the relative IHC scores for UFL1 and DDRGK1. Statistical analysis was performed via an unpaired two-sided Student's t-test. *P < 0.05, ***P < 0.00, ****P < 0.00, ***P < 0.00, *

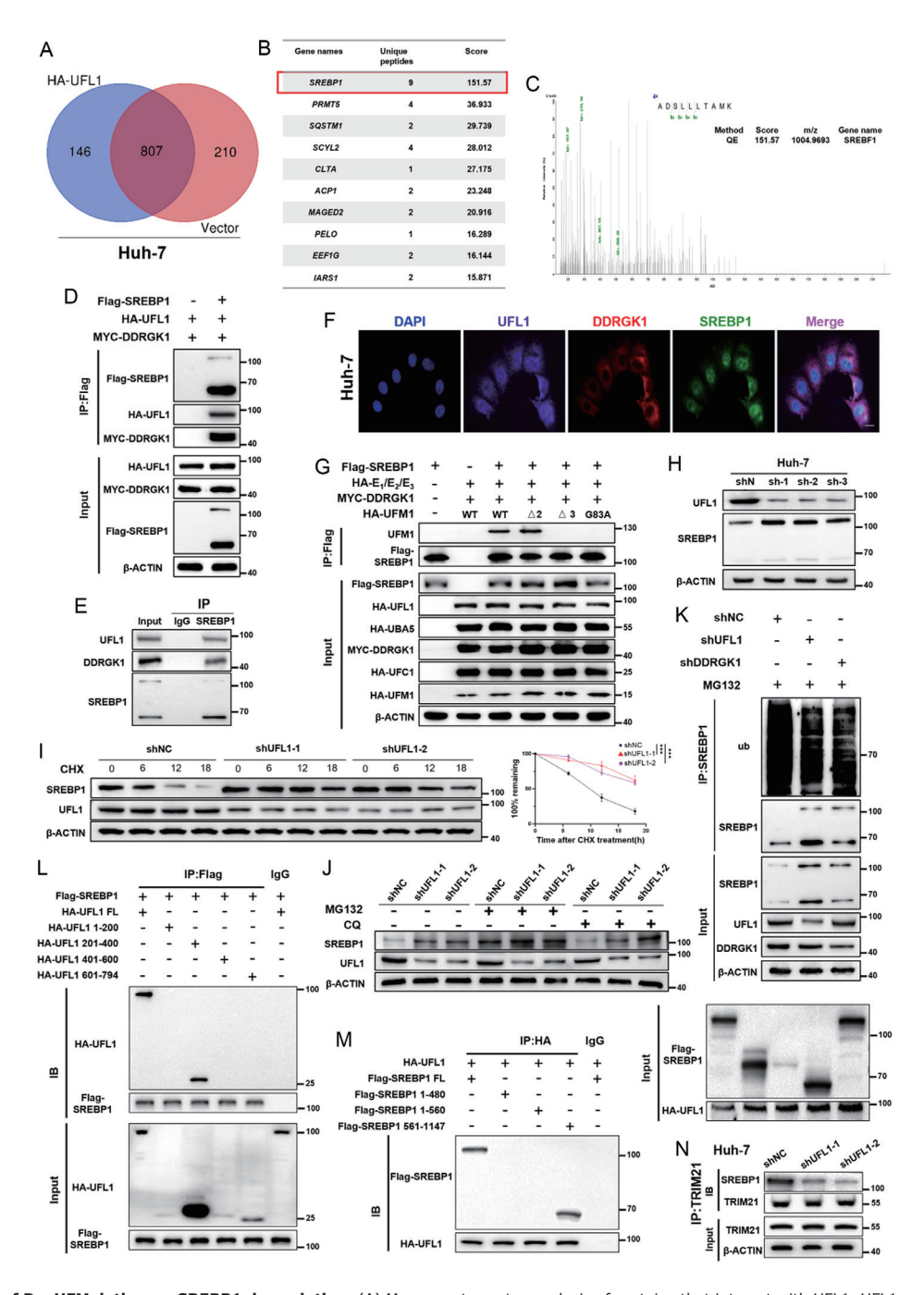


Fig. 2. The impact of DysUFMylation on SREBP1 degradation. (A) Mass spectrometry analysis of proteins that interact with UFL1. UFL1 was immunoprecipitated from the lysates of Huh-7 cells expressing HA-UFL1 or vector. The immunoprecipitates were subjected to mass spectrometry analysis. (B) List of the top ten proteins among the 146 unique proteins that interact with UFL1 according to mass spectrometry analysis. (C) Peptide spectrum of SREBP1 identified by mass spectrometry in the immunoprecipitates of HA-UFL1. (D) Western blot analysis of the interactions between SREBP1, UFL1, and DDRGK1 in HEK293T cells expressing HA-UFL1, MYC-DDRGK1, and Flag-SREBP1 via co-immunoprecipitation with an anti-Flag antibody. (E) Western blot analysis of the interactions between UFL1, DDRGK1, and SREBP1 in Huh-7 cells, conducted via co-immunoprecipitation with an SREBP1 antibody. IgG was used as a control. (F) Immunofluorescence image of the colocalization of UFL1 and DDRGK1 with SREBP1 in Huh-7 cells. Scale bar, 5 µm. (G) UFMylation of SREBP1 was analyzed by Western blotting with an anti-UFM1 antibody in HEK293T cells expressing components of the UFMylation system. UFM1^{AC2} and UFM1^{AC3} were chosen as active and defective UFM1 variants, respectively, whereas UFM1^{G83A} represents a mutation in which Gly83 of HA-UFM1 was changed to Ala. (H) Western blot analysis of SREBP1 expression in Huh-7 cells following UFL1 knockdown. (I) SREBP1 stability was compared between UFL1-knockdown Huh-7 cells and control cells. The cells were treated with 100 µg/mL cycloheximide (CHX) for the indicated times. Data are representative of three independent experiments. (J) UFL1 knockdown cells were treated with MG132 (20 µM) or CQ (100 µM) for the indicated times, followed by Western blot analysis with an anti-SREBP1 antibody. Data are representative of three independent experiments. (K) Ubiquitination of endogenous SREBP1 was analyzed by immunoprecipitation using an SREBP1 antibody, followed by Western blot analysis in Huh-7 cells with UFL1 or DDRGK1 knockdown in the presence of MG132 (20 µM). Data are representative of three independent experiments. (L, M) Western blot analysis of the binding domains between UFL1 and SREBP1. (N) After knockdown of UFL1 in Huh-7 cells, the level of TRIM21-bound SREBP1 was measured by Western blot. IP, Immunoprecipitation; E1, UBA5; E2, UFC1; E3, UFL1; CHX, cycloheximide; CQ, Chloroquine; IB, Immunoblotting; +, with; -, without.

degradation of SREBP1 (Fig. 2J and Supplementary Fig. 1J). Indeed, the ubiquitination of SREBP1 was significantly reduced following the knockdown of UFL1 or DDRGK1 in Huh-7 cells (Fig. 2K). Here, we further characterized the domains required for the interaction between UFL1 and SREBP1 and revealed that residues 200-400 of UFL1 and residues 561-1147 of SREBP1 are critical for their interaction (Fig. 2L and M). Moreover, prior studies have reported that Tripartite motif-containing protein 21 (TRIM21) promotes the ubiquitin-mediated degradation of SREBP1.⁴⁸ Therefore, we investigated whether UFL1 regulates the ubiquitination of SREBP1 in a TRIM21-dependent manner. Our results demonstrate that knockdown of UFL1 significantly reduces the binding of SREBP1 to TRIM21, indicating that UFL1-mediated UFMylation is essential for TRIM21-dependent ubiquitination of SREBP1 (Fig. 2N and Supplementary Fig. 1K). Collectively, these data suggest that dysregulation of UFMylation promotes SREBP1 stability by antagonizing TRIM21-mediated ubiquitination.

Dysregulation of UFMylation in SREBP1 enhances its downstream lipid metabolism

SREBP1 is a critical transcription factor involved in lipid metabolism.⁴⁹ Therefore, we sought to identify the downstream changes associated with SREBP1. First, we observed that the levels of enzymes downstream of SREBP1, including Stearoyl-Coenzyme A Desaturase 1 (SCD1), ATP-citrate lyase (ACLY), Acetyl-CoA Carboxylase 1 (ACC1), and Fatty Acid Synthase (FASN), increased following the knockdown of UFL1 or DDRGK1 (Fig. 3A and B; Supplementary Fig. 2A and B). We subsequently performed Oil Red O and Nile Red staining to observe changes in lipid levels within the cells. We found that the knockdown of UFL1 or DDRGK1 increased the lipid content in both Huh-7 and HepG2 cells, and this effect was partially offset by the knockdown of SREBP1 (Fig. 3C and D; Supplementary Fig. 2C). Furthermore, we used assay kits to measure the intracellular levels of TG, CHOL, and FFA, all of which were significantly increased, and this increase was attenuated by SREBP1 knockdown (Fig. 3E and Supplementary Fig. 2D). To investigate whether this phenomenon occurs within tissue, we conducted immunohistochemistry and Oil Red O staining on HCC tissue samples. The results indicated that patients with low expression of UFL1 and DDRGK1 had higher levels of SREBP1 and lipids, and vice versa (Fig. 3F). In addition, we measured the levels of TG, CHOL, and FFA in 30 HCC tissues, and our Western blot results revealed that UFL1 and DDRGK1 in HCC tissues were negatively correlated with SREBP1 and lipid contents (Fig. 3G and Supplementary Fig. 2E). Moreover, our TMA results further confirmed that UFL1 and DDRGK1 are negatively correlated with SREBP1 in HCC (Supplementary Fig. 2F). Taken together, our findings suggest that following the knockdown of UFL1 or DDRGK1, SREBP1 becomes more stable, thereby enhancing downstream lipid metabolism.

The decrease in UFMylation levels to promote HCC progression is SREBP1-dependent in vitro

According to previous reports, accumulated lipids can promote tumor growth and metastasis. ^{23,50,51} Therefore, we aimed to determine whether the knockdown of UFL1 or DDRGK1 could promote tumor cell progression. Our colony formation assays demonstrated that the knockdown of UFL1 or DDRGK1 promoted the proliferation of Huh-7 and HepG2 cells. Moreover, this proliferation-promoting effect was counteracted by SREBP1 knockdown (Fig. 4A and Supplementary Fig. 3A). The results of the EdU assay were similar (Fig. 4B and Supplementary Fig. 3B). The knockdown efficiency of

SREBP1 was verified by Western blotting (Supplementary Fig. 3C). To assess cell migration and invasion abilities, we conducted wound healing and Transwell assays. The results showed that after UFL1 or DDRGK1 was knocked down, cell migration and invasion abilities were enhanced, but these effects were counteracted by SREBP1 knockdown (Fig. 4C and D; Supplementary Fig. 3D and E). These data suggest that SREBP1 is critical for HCC cell growth and metastasis *in vitro* after UFL1 or DDRGK1 knockdown.

Knockdown of UFL1 or DDRGK1 promotes HCC cell growth and metastasis through SREBP1-related lipid metabolism in vivo

To further investigate the impact of UFL1 or DDRGK1 knockdown on HCC development, we established an orthotopic tumor model in nude mice. Similar to the results of the cell experiments, the knockdown of UFL1 or DDRGK1 significantly promoted HCC growth, and this effect was at least partially neutralized by the knockdown of SREBP1 (Fig. 5A and B; Supplementary Fig. 4A and B). Accordingly, immunohistochemical staining of tumor tissues revealed that, when UFL1 or DDRGK1 was knocked down, the expression of SREBP1 increased (Fig. 5C). Oil Red O staining further corroborated these findings (Fig. 5C). Further studies revealed that the levels of TG, CHOL, and FFA in tumors increased after UFL1 or DDRGK1 was knocked down, and this increase was partially blocked by SREBP1 knockdown (Fig. 5D). To determine the effect of dysUFMylation on HCC metastasis in vivo, we constructed a lung metastasis model in nude mice. The results indicated that dysUFMylation promoted lung metastasis in HCC, and knockdown of SREBP1 partially reversed this pro-metastatic effect (Fig. 5E).

Taken together, these data suggest that dysUFMylation promotes the growth and metastasis of HCC in an SREBP1-dependent manner.

Targeting SREBP1 can enhance the efficacy of lenvatinib in HCC patients with low UFL1 expression

Research suggests that lenvatinib, as a first-line treatment, may be noninferior to combination therapy with immune checkpoint inhibitors. 52 However, many patients develop drug resistance, and the mechanisms involved are multifaceted. Reports indicate that CHOL biosynthesis supports the expansion of cancer stem cell populations to drive resistance to tyrosine kinase inhibitor therapy in hepatocellular carcinoma, and the combined use of Fatostatin and lenvatinib has a higher treatment efficacy when SLP2 is highly expressed. 53,54 Therefore, we aimed to investigate whether targeting SREBP1 and inhibiting lipogenesis could increase the efficacy of lenvatinib in the context of UFL1 knockdown. Fatostatin is an SREBP1 inhibitor that prevents the translocation of SREBP1 to the nucleus, thereby blocking its activation process and inhibiting lipogenesis. Dosing begins one week after the establishment of orthotopic xenografts, with a strategy that includes fatostatin monotherapy, lenvatinib monotherapy, and a combination of fatostatin and lenvatinib (Fig. 6A). Our orthotopic xenograft results indicated that fatostatin mitigated the protumor effects associated with UFL1 knockdown. Moreover, when combined with lenvatinib, tumor growth was effectively controlled (Fig. 6B and Supplementary Fig. 4C). In addition, fatostatin weakened lung metastasis caused by UFL1 knockdown, and the combination of fatostatin and lenvatinib further reduced lung metastasis in this context (Fig. 6C). In summary, dysUFMylation of SREBP1 enhances its protein stability, thereby promoting downstream fatty acid synthesis and ultimately driving tumor progression (Fig. 6D).

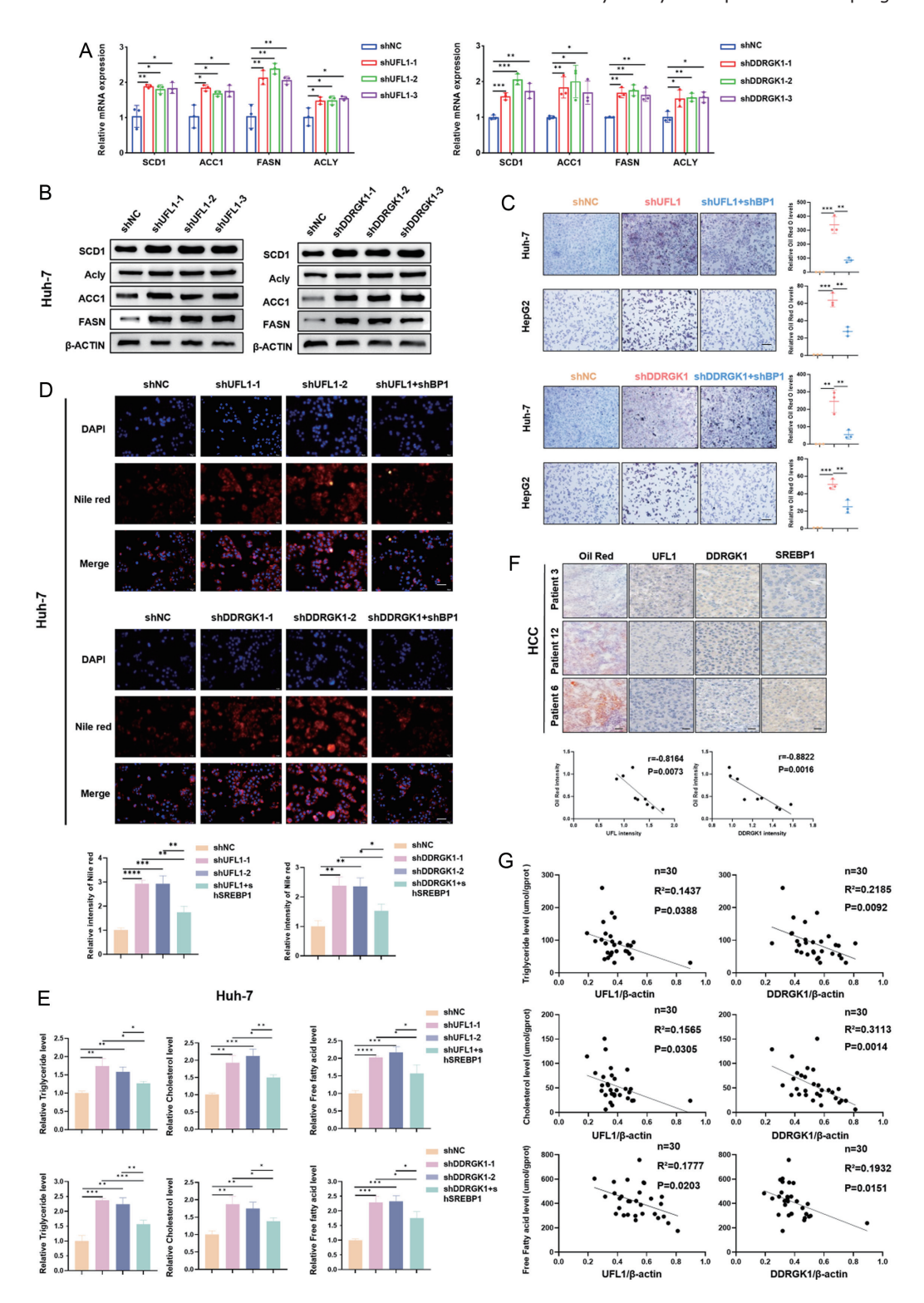


Fig. 3. The effects of SREBP1 DysUFMylation on downstream lipid metabolism. (A) The mRNA levels of SCD1, ACC1, FASN, and ACLY were measured after UFL1 or DDRGK1 was knocked down in Huh-7 cells. (B) The protein levels of SCD1, ACC1, FASN, and ACLY were assessed after UFL1 or DDRGK1 was knocked down in Huh-7 cells. (C) Oil Red O staining of Huh-7 and HepG2 cells in the indicated groups. Scale bar, 20 μ m. Data are representative of three independent experiments. (D) Nile red staining of Huh-7 cells in the indicated groups. Scale bar, 10 μ m. Data are representative of three independent experiments. (E) The levels of triglyceride (TG), cholesterol (CHOL), and free fatty acids (FFA) in Huh-7 cells in the indicated groups. n = 3. Data are representative of three independent experiments. (F) Representative sections from corresponding patients subjected to immunohistochemical staining for UFL1, DDRGK1, and SREBP1, along with Oil Red O staining. Statistical analysis of the correlation between UFL1 or DDRGK1 and Oil Red. Scale bars, 10 μ m (left) and 5 μ m (right). (G) Levels of TG, CHOL, and FFA in relation to UFL1 and DDRGK1 expression in 30 HCC patients. *P < 0.05, **P < 0.05, **P < 0.01, ***P < 0.001, ****P < 0.001, ***

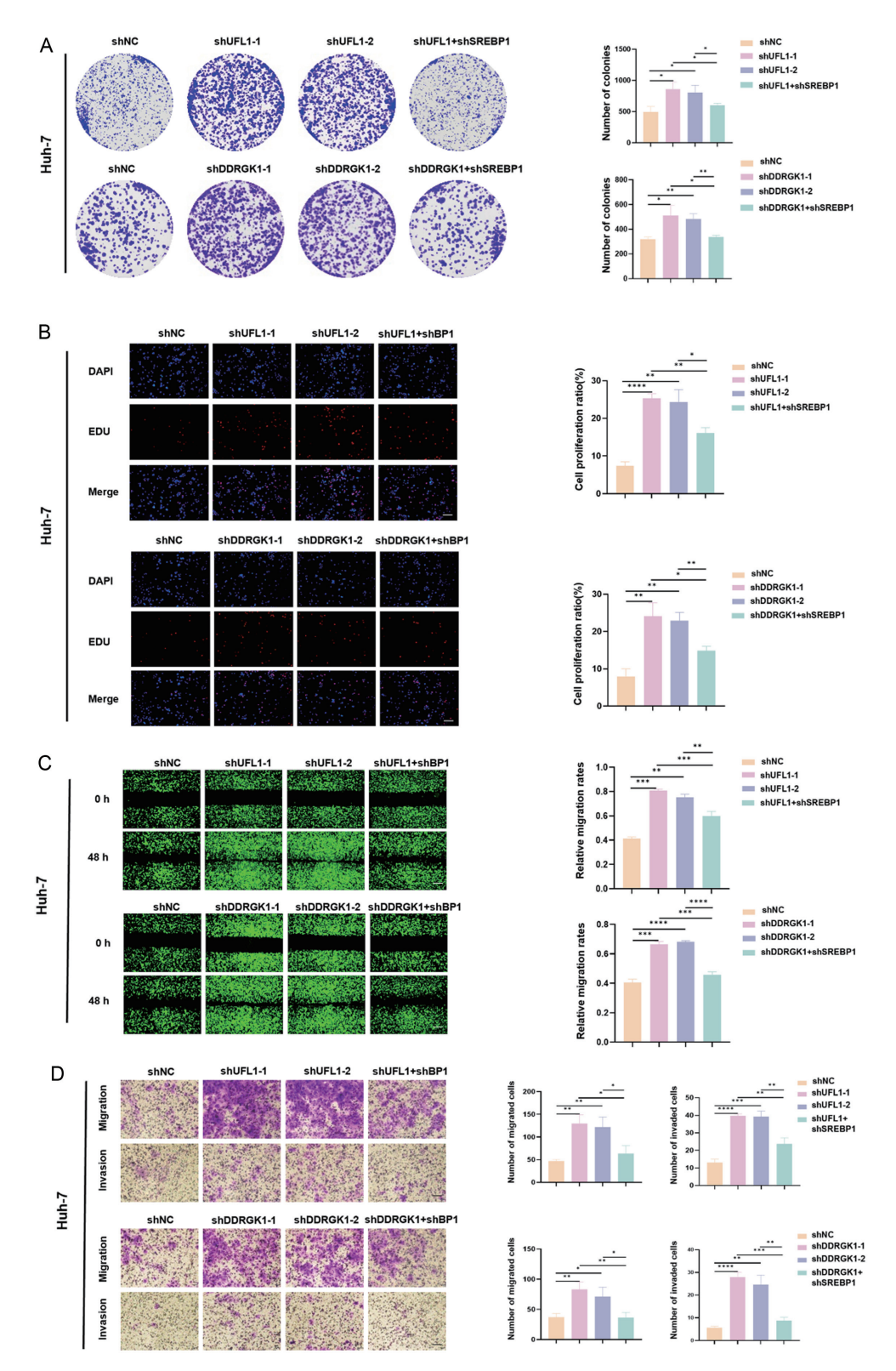


Fig. 4. The effects of UFL1 or DDRGK1 knockdown on the *in vitro* growth and metastasis of HCC. (A) Colony formation assay of Huh-7 cells following knockdown of UFL1 or DDRGK1. A rescue assay was conducted by subsequently knocking down SREBP1. Data are representative of three independent experiments. (B) EdU assay of Huh-7 cells following knockdown of UFL1 or DDRGK1. Scale bar, 20 μm. Data are representative of three independent experiments. (C) Wound-healing assay of Huh-7 cells following knockdown of UFL1 or DDRGK1. Scale bar, 50 μm. Data are representative of three independent experiments. (D) Transwell migration and invasion assays of Huh-7 cells following knockdown of UFL1 or DDRGK1. Scale bar, 10 μm. Data are representative of three independent experiments. *P < 0.05, **P < 0.01, ***P < 0.001, ****P < 0.001. ***P < 0.0001. EDU, 5-Ethynyl-2′-deoxyuridine; HCC, hepatocellular carcinoma.

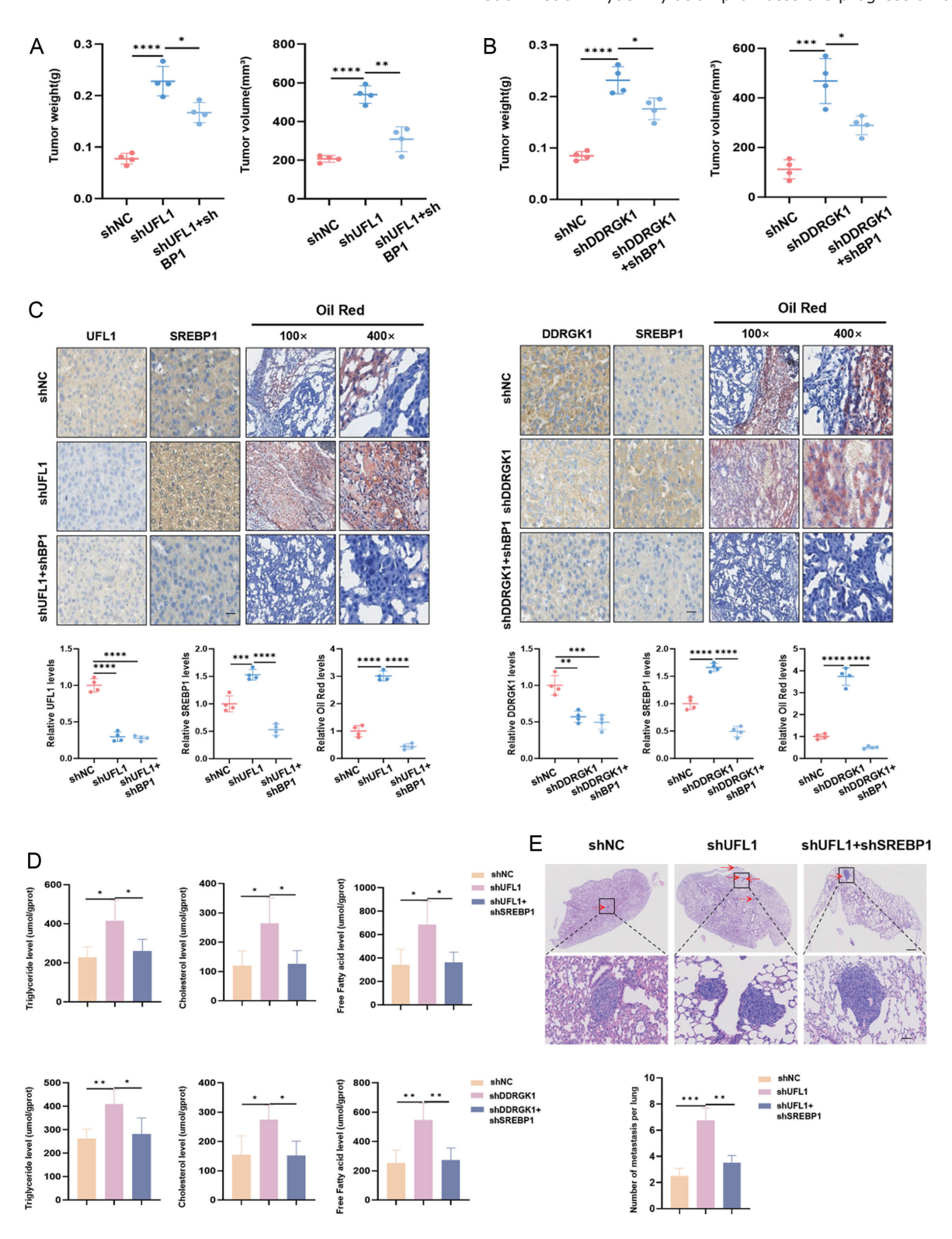


Fig. 5. The effects of UFL1 or DDRGK1 knockdown on HCC growth and metastasis *in vivo*. (A, B) Tumor volume and weight were measured in the indicated groups. The data were analyzed via unpaired Student's t-tests (n = 4 for each experimental group). (C) Immunohistochemistry of UFL1, DDRGK1, and SREBP1 in tumor sections as described in (A, B). Oil Red O staining of the indicated tumors. Statistical analysis of the levels of UFL1, DDRGK1, SREBP1, and Oil Red corresponding groups. Scale bar, 5 μm. (D) Levels of TG, CHOL, and FFA in the tumors described above. Data are representative of three independent experiments. n = 4. (E) Microscopy images of lung metastases in mice injected with the indicated cells (n = 4 for each experimental group). The lung sections were stained with H&E. The number of metastatic nodules in individual mice was determined via microscopy. Scale bars, 50 μm (top) and 10 μm (bottom). *P < 0.05, **P < 0.01, ****P < 0.001, ****P < 0.001. HCC, hepatocellular carcinoma.

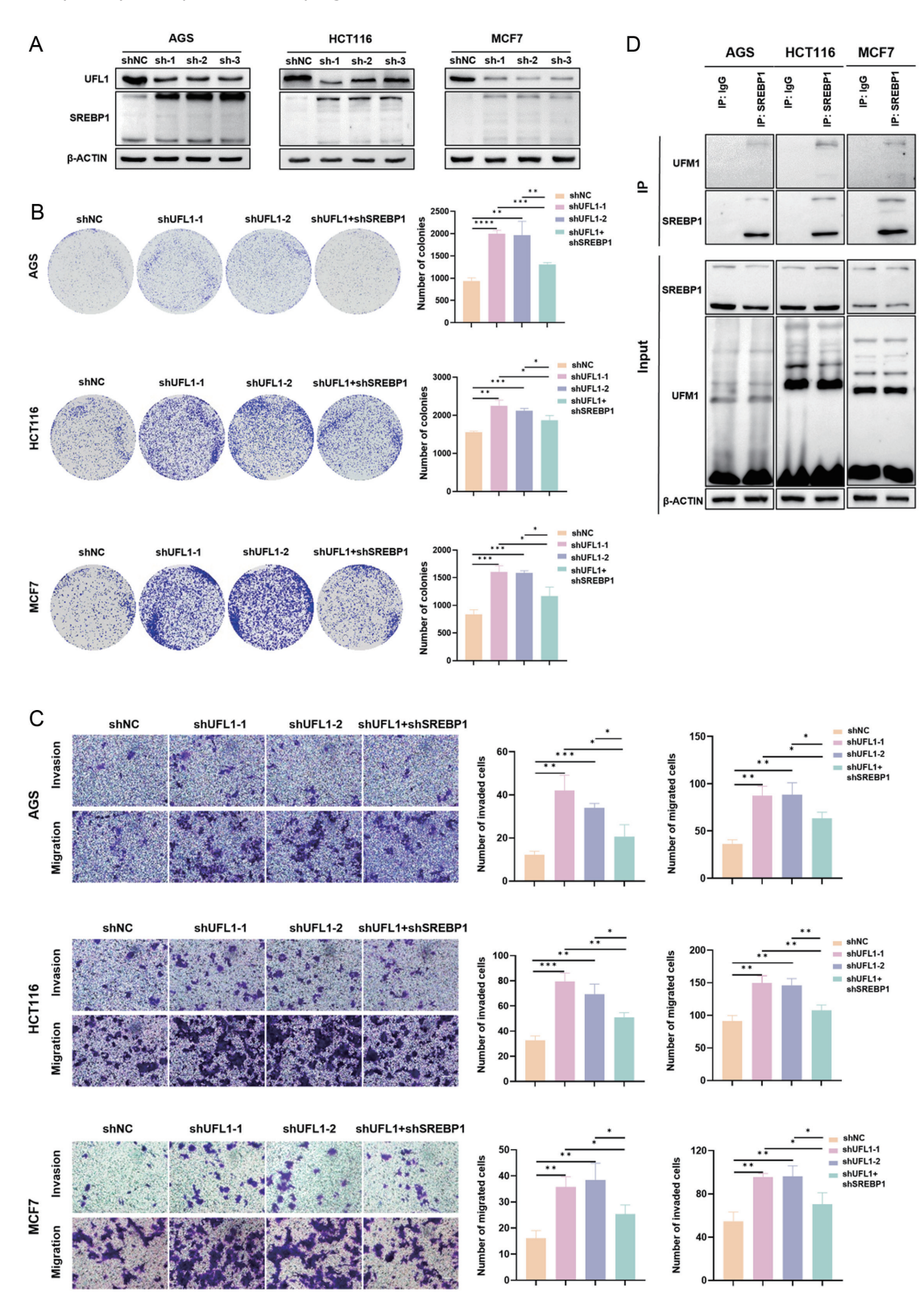


Fig. 6. The effects of the combination of SREBP1 inhibitor with lenvatinib in HCC. (A) Workflow for the construction of the HCC orthotopic mouse model. (B) Tumor volume and weight in the indicated groups (n = 4 for each experimental group). (C) Microscopy images of lung metastases in mice from different groups. The lung sections were stained with H&E, and the number of metastatic nodules in individual mice was determined via microscopy (n = 4 for each experimental group). (D) Schematic diagram of the proposed model of UFMylation in HCC progression. *P < 0.05, **P < 0.01, ****P < 0.001, ****P < 0.0001. HCC, hepatocellular carcinoma; i.g., intragastric administration; i.p., intraperitoneal injection; qd, once a day; tiw, three times a week.

Additionally, fatostatin can synergize with lenvatinib in HCC patients with low UFL1 expression.

DysUFMylation promotes AGS, HCT116, and MCF7 cell proliferation, migration, and invasion via SREBP1

We have demonstrated that dysUFMylation can promote tumor progression through SREBP1 in HCC. Thus, we aimed to explore whether this phenomenon also occurs in other tumor types. AGS, HCT116, and MCF7 cells were selected for this investigation. The results indicated that UFL1 knockdown induces the accumulation of SREBP1 (Fig. 7A). In addition, phenotypic experiments confirmed that UFL1 knockdown promotes the proliferation, migration, and invasion abilities of these cells, and this promotion can be attenuated by SREBP1 knockdown (Fig. 7B and C). To further investigate whether SREBP1 is subject to UFMylation, similar to what we observed in HCC, we conducted coimmunoprecipitation and obtained consistent results (Fig. 7D).

Collectively, these findings suggest that dysUFMylation promotes cancer progression via SREBP1 in various tumor types, including but not limited to hepatocellular carcinoma, gastric adenocarcinoma, colorectal carcinoma, and breast cancer.

Discussion

The present study establishes a direct mechanistic link between UFMylation and lipid metabolism in cancer. Although UFMvlation has been implicated in diverse physiological processes such as endoplasmic reticulum homeostasis, hematopoiesis, and embryonic development, its contribution to tumor biology has remained insufficiently characterized. Here, we propose that UFMylation acts as a critical regulator of lipid metabolism by controlling the stability of SREBP1, a master transcriptional factor of lipogenesis. This is consistent with the previously reported role of UFMylation.⁶ The functional significance of this regulation is highlighted by the central role of lipid metabolism in tumor development. Accumulated evidence suggests that aberrant lipogenesis contributes to immune evasion and therapeutic resistance. 20,55 This finding integrates two essential aspects of tumorigenesis, posttranslational modification and metabolic reprogramming, into a unifying model. The mechanism illustrates how ubiquitinlike modifiers may serve not simply as independent signals but as regulatory layers that interface with ubiquitination to fine-tune protein stability. Moreover, the identification of SREBP1 as a UFMylation substrate expands the catalog of known targets, which already includes immune checkpoint molecules such as programmed cell death protein 1 and programmed cell death 1 ligand 1, as well as tumor suppressors like tumor protein 53.6,7,9 This suggests that UFMylation may intersect with diverse oncogenic and immunologic pathways, with implications extending beyond metabolism. Understanding how UFMylation selects its substrates and whether distinct cofactors direct its specificity are important questions for future research.

Importantly, single-cell transcriptomic and multi-omic approaches could refine our understanding of how the SREBP1–UFMylation axis operates within heterogeneous HCC. scRNA-seq may identify hepatocyte subpopulations with differential UFMylation activity and distinct SREBP1-driven metabolic programs, while spatial transcriptomics could reveal how these cells interact with immune or stromal compartments. Integration with single-cell ATAC-seq may further uncover cell type-specific chromatin changes downstream of UFMylation. Together, these approaches would validate our model at

single-cell resolution and highlight therapeutic vulnerabilities masked in bulk analyses.

Our findings also offer translational implications. Therapeutic strategies targeting the UFMylation-SREBP1 axis may enhance the efficacy of existing therapies and provide an avenue to overcome drug resistance. In addition, recent evidence suggests that panaxatriol may function as an agonist of UFL1⁵⁶; therefore, we speculate that pharmacological activation of UFL1 by panaxatriol could potentially suppress tumor progression, and its combination with lenvatinib warrants further exploration as an intriguing therapeutic strategy.

Nevertheless, our study has certain limitations. Although we demonstrated the role of UFMylation in regulating SREBP1 stability, the precise molecular mechanism by which UFMylation facilitates TRIM21 binding warrants further structural and biochemical investigation. In addition, while fatostatin served as a proof-of-concept inhibitor, more specific and clinically applicable SREBP1 inhibitors are needed to validate the therapeutic potential of targeting this pathway. Furthermore, our study primarily focused on the UFL1-DDRGK1 complex, but whether other UFMylation components or substrates contribute to HCC progression remains to be explored. Finally, clinical validation in larger patient cohorts is required to establish UFMylation as a prognostic marker and therapeutic target.

Conclusions

Our study uncovers a novel regulatory mechanism at the intersection of UFMylation and lipid metabolism, provides new insights into the metabolic vulnerabilities of HCC, and suggests that targeting the UFMylation-SREBP1 axis could be a promising therapeutic strategy for HCC and potentially other cancers.

Funding

This study was supported by grants from the National Natural Science Foundation of China (82472816 and 82103521 to CZ, 82072672 to YY, 82472804 to NR), the Natural Science Foundation of Shanghai (25ZR1401061), the Sino-German Mobility Program (M-0603), and the Shanghai "Rising Stars of Medical Talents" Youth Development Program (SHWSRS(2024)070).

Conflict of interest

This paper has been uploaded to ResearchSquare as a preprint: https://www.researchsquare.com/article/rs-5305970/ v1, The other authors have no conflict of interests related to this publication.

Author contributions

Experiment design and performance, writing of the manuscript (XG, MX, ZH), data analysis (ZW, HX), patient tissue sample supply, clinical data analysis (SQ, NR, CZ, YY), animal model establishment (XG, GS, DZ), the entire project supervision, experiment design, and revision of the manuscript (YY, CZ). All authors have approved the final version and publication of the manuscript.

Ethical statement

All procedures performed in this study involving human participants followed the ethical standards of the Clinical Re-

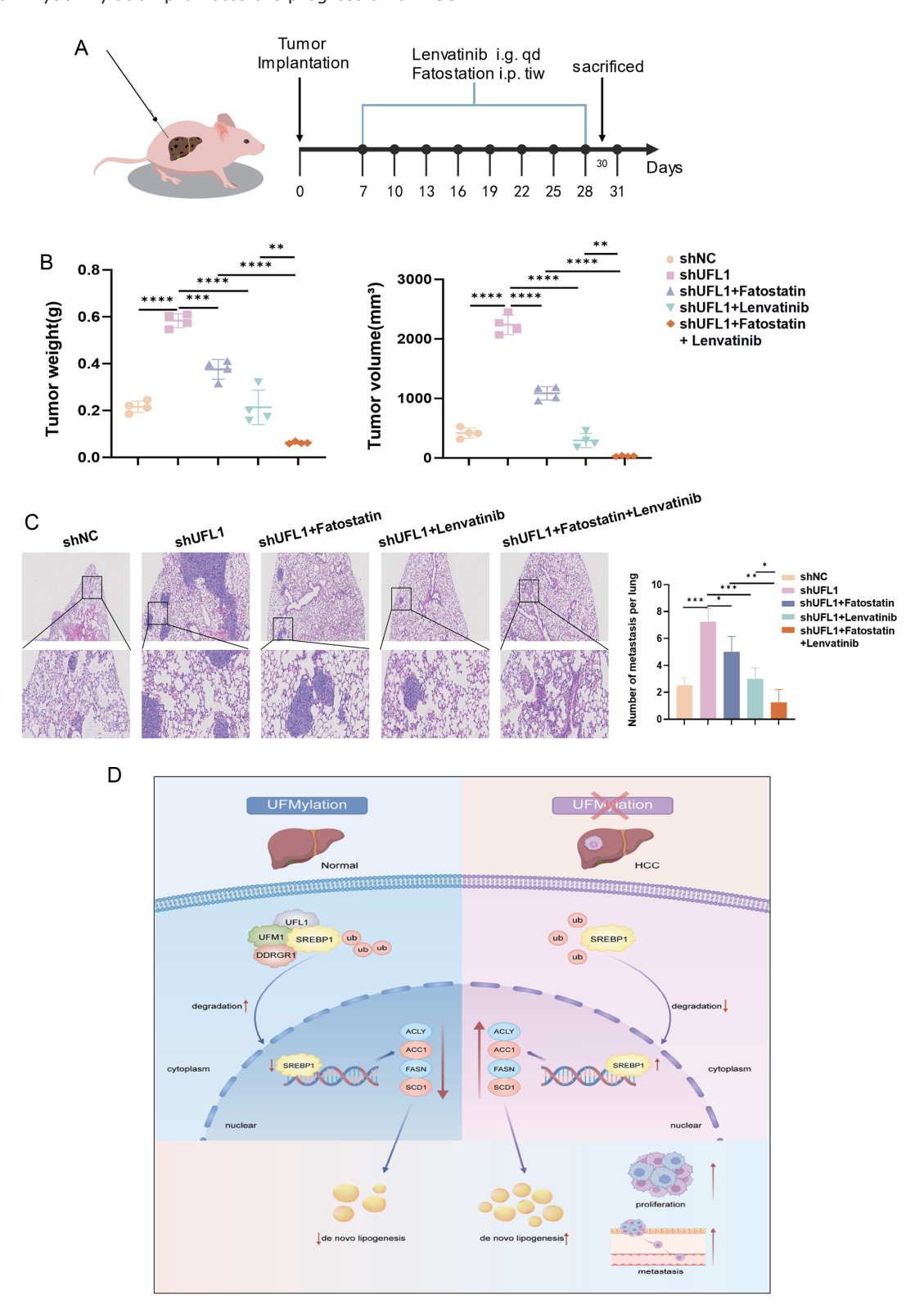


Fig. 7. Effects of DysUFMylation on proliferation, migration, and invasion in AGS, HCT116, and MCF7 cells. (A) Western blot analysis of SREBP1 protein levels in AGS, HCT116, and MCF7 cells following UFL1 knockdown. (B) Colony formation assay of AGS, HCT116, and MCF7 cells following UFL1 knockdown. Data are representative of three independent experiments. (C) Transwell migration and invasion assays of AGS, HCT116, and MCF7 cells following UFL1 knockdown. Scale bar, 10 µm. Data are representative of three independent experiments. (D) UFMylation of endogenous SREBP1 was analyzed by immunoprecipitation using an SREBP1 antibody, followed by Western blotting with an anti-UFM1 antibody in AGS, HCT116, and MCF7 cells in the presence of MG132. Created with BioRender. *P < 0.05, **P < 0.01, ****P < 0.001. ****P < 0.0001.

search Ethics Committee of Zhongshan Hospital, Fudan University (B2021-143R) and the 2024 Helsinki Declaration and its later amendments or comparable ethical standards. The authors have obtained verbal and written informed consent from the patient for inclusion in the study. The animal experiments were approved by the Institutional Animal Care and Use Committee of Zhongshan Hospital, Fudan University (2024-034). All animals received human care.

Data sharing statement

The datasets generated and analyzed during the current study are available from the corresponding author on reasonable request.

References

- [1] Bray F, Laversanne M, Sung H, Ferlay J, Siegel RL, Soerjomataram I, et al. Global cancer statistics 2022: GLOBOCAN estimates of incidence and mortality worldwide for 36 cancers in 185 countries. CA Cancer J Clin 2024;74(3):229–263. doi:10.3322/caac.21834, PMID:38572751.
- Chen QF, Chen S, Chen M, Lyu N, Zhao M. Improving the Conversion Success Rate of Hepatocellular Carcinoma: Focus on the Use of Combination Therapy with a High Objective Response Rate. J Clin Transl Hepatol 2024;12(3):298–304. doi:10.14218/JCTH.2023.00403, PMID:38426191.
- Mao Z, Ma X, Jing Y, Shen M, Ma X, Zhu J, et al. Ufmylation on UFBP1 alleviates non-alcoholic fatty liver disease by modulating hepatic endoplasmic reticulum stress. Cell Death Dis 2023;14(9):584. doi:10.1038/s41419-023-06095-2, PMID:37660122. Komatsu M, Chiba T, Tatsumi K, Iemura S, Tanida I, Okazaki N, *et al*.
- A novel protein-conjugating system for Ufm1, a ubiquitin-fold modifier. EMBO J 2004;23(9):1977–1986. doi:10.1038/sj.emboj.7600205,
- PMID:15071506.

 Tatsumi K, Sou YS, Tada N, Nakamura E, Iemura S, Natsume T, et al. A novel type of E3 ligase for the Ufm1 conjugation system. J Biol Chem 2010;285(8):5417–5427. doi:10.1074/jbc.M109.036814, PMID:20018847. Zhou J, Ma X, He X, Chen B, Yuan J, Jin Z, et al. Dysregulation of PD-L1 by UFMylation imparts tumor immune evasion and identified as a potential
- by OffMylation impairs tumor immune evasion and identified as a potential therapeutic target. Proc Natl Acad Sci U S A 2023;120(11):e2215732120. doi:10.1073/pnas.2215732120, PMID:36893266. Liu J, Guan D, Dong M, Yang J, Wei H, Liang Q, et al. UFMylation maintains tumour suppressor p53 stability by antagonizing its ubiquitination. Nat Cell Biol 2020;22(9):1056–1063. doi:10.1038/s41556-020-0559-z, PMID:32072031 PMID:32807901.
- Qin B, Yu J, Nowsheen S, Wang M, Tu X, Liu T, et al. UFL1 promotes histone H4 ufmylation and ATM activation. Nat Commun 2019;10(1):1242. doi:10.1038/s41467-019-09175-0, PMID:30886146. He C, Xing X, Chen HY, Gao M, Shi J, Xiang B, et al. UFL1 ablation in T cells suppresses PD-1 UFMylation to enhance anti-tumor immunity.
- Mol Cell 2024;84(6):1120-1138.e8. doi:10.1016/j.molcel.2024.01.024, PMID:38377992
- $[10] \ Wu\ J, Lei\ G, Mei\ M, Tang\ Y, Li\ H.\ A\ novel\ C53/LZAP-interacting\ protein\ regulates$
- stability of C53/LZAP and DDRGK domain-containing Protein 1 (DDRGK1) and modulates NF-kappaB signaling. J Biol Chem 2010;285(20):15126–15136. doi:10.1074/jbc.M110.110619, PMID:20228063.

 [11] DaRosa PA, Penchev I, Gumbin SC, Scavone F, Wąchalska M, Paulo JA, et al. UFM1 E3 ligase promotes recycling of 60S ribosomal subunits from the ER. Nature 2024;627(8003):445–452. doi:10.1038/s41586-024-07073-0, PMID:38383785 PMID: 38383785
- [12] Zhou X, Mahdizadeh SJ, Le Gallo M, Eriksson LA, Chevet E, Lafont E. UF-Mylation: a ubiquitin-like modification. Trends Biochem Sci 2024;49(1):52–67. doi:10.1016/j.tibs.2023.10.004, PMID:37945409.
- 67. doi:10.1016/j.tibs.2023.10.004, PMID:37945409.
 [13] Cai Y, Pi W, Sivaprakasam S, Zhu X, Zhang M, Chen J, et al. UFBP1, a Key Component of the Ufm1 Conjugation System, Is Essential for Ufmylation-Mediated Regulation of Erythroid Development. PLoS Genet 2015;11(11):e1005643. doi:10.1371/journal.pgen.1005643, PMID:26544067.
 [14] Makhlouf L, Peter JJ, Magnussen HM, Thakur R, Millrine D, Minshull TC, et al. The UFM1 E3 ligase recognizes and releases 60S ribosomes from ER translocons. Nature 2024;627(8003):437–444. doi:10.1038/s41586-024-07082-wp.PMID:38383789
- 07093-w, PMID:38383789. [15] Ishimura R, El-Gowily AH, Noshiro D, Komatsu-Hirota S, Ono Y, Shindo M,
- et al. The UFM1 system regulates ER-phagy through the ufmylation of CY-B5R3. Nat Commun 2022;13(1):7857. doi:10.1038/s41467-022-35501-0, PMID:36543799 [16] Patel CH, Leone RD, Horton MR, Powell JD. Targeting metabolism to regu-
- late immune responses in autoimmunity and cancer. Nat Rev Drug Discov 2019;18(9):669–688. doi:10.1038/s41573-019-0032-5, PMID:31363227
- Martínez-Reyes I, Chandel NS. Cancer metabolism: looking forward. Nat Rev Cancer 2021;21(10):669–680. doi:10.1038/s41568-021-00378-6,
- Rev Cancer 2021;21(10):009-000. doi:10.1036,5.11 PMID:34272515. [18] You M, Xie Z, Zhang N, Zhang Y, Xiao D, Liu S, et al. Signaling pathways in cancer metabolism: mechanisms and therapeutic targets. Signal Transduct Target Ther 2023;8(1):196. doi:10.1038/s41392-023-01442-3,
- [19] Mossmann D, Müller C, Park S, Ryback B, Colombi M, Ritter N, et al. Arginine

- reprograms metabolism in liver cancer via RBM39. Cell 2023;186(23):5068-
- 5083.e23. doi:10.1016/j.cell.2023.09.011, PMID:37804830. [20] De Martino M, Rathmell JC, Galluzzi L, Vanpouille-Box C. Cancer cell me-
- [20] De Martino M, Rathmell JC, Galluzzi L, Vanpouille-Box C. Cancer cell metabolism and antitumour immunity. Nat Rev Immunol 2024;24(9):654–669. doi:10.1038/s41577-024-01026-4, PMID:38649722.
 [21] Calvisi DF, Wang C, Ho C, Ladu S, Lee SA, Mattu S, et al. Increased lipogenesis, induced by AKT-mTORC1-RPS6 signaling, promotes development of human hepatocellular carcinoma. Gastroenterology 2011;140(3):1071–1083. doi:10.1053/j.gastro.2010.12.006, PMID:21147110.
 [22] Martin-Perez M, Urdiroz-Urricelqui U, Bigas C, Benitah SA. The role of lipids in cancer progression and metatoris. Coll Matta 2023;34(11):1675–61.
- pids in cancer progression and metastasis. Cell Metab 2022;34(11):1675–1699. doi:10.1016/j.cmet.2022.09.023, PMID:36261043.

 [23] Li C, Yang W, Zhang J, Zheng X, Yao Y, Tu K, et al. SREBP-1 has a prognostic role and contributes to invasion and metastasis in human hepatocellular carcinoma. Int J Mol Sci 2014;15(5):7124–7138. doi:10.3390/ijms15057124, PMID:24776759.
- [24] Jia Y, Yan Q, Zheng Y, Li L, Zhang B, Chang Z, et al. Long non-coding RNA NEAT1 mediated RPRD1B stability facilitates fatty acid metabolism and lymph node metastasis via c-Jun/c-Fos/SREBP1 axis in gastric cancer. J Exp Clin Cancer Res 2022;41(1):287. doi:10.1186/s13046-022-02449-4, PMID:36171622.
- [25] Zhou C, Qian W, Li J, Ma J, Chen X, Jiang Z, et al. High glucose microenvi-ronment accelerates tumor growth via SREBP1-autophagy axis in pancreatic cancer. J Exp Clin Cancer Res 2019;38(1):302. doi:10.1186/s13046-019-1288-7, PMID:31296258.
- [26] Zhou C, Chen W, Sun J, Atyah M, Yin Y, Zhang W, et al. Low expression of WW domain-containing oxidoreductase associates with hepatocellular carcinoma aggressiveness and recurrence after curative resection. Cancer
- Med 2018; 7(7):3031-3043. doi:10.1002/cam4.1591, PMID:29905011. [27] Liu Y, Yang T, Wei YW. What is the difference between overall survival, recur-
- [27] Liu Y, Yang I, Wei YW. What is the difference between overall survival, recurrence-free survival and time-to-recurrence? Br J Surg 2020;107(12):e634. doi:10.1002/bjs.11945, PMID:32955103.
 [28] Segeritz C-P, Vallier L. Cell Culture. Basic Science Methods for Clinical Researchers. Salt Lake City, UT: Academic Press; 2017:151–172.
 [29] Aranda A, Bezunartea J, Casales E, Rodriguez-Madoz JR, Larrea E, Prieto J, et al. A quick and efficient method to generate mammalian stable cell lines based on a novel inducible alphavirus DNA/RNA layered system. Cell Mol Life Sci 2014;71(23):4637–4651. doi:10.1007/s00018-014-1631-2, PMID:24794511. PMID:24794511.
- [30] Kurien BT, Scofield RH. Western blotting. Methods 2006;38(4):283–293. doi:10.1016/j.ymeth.2005.11.007, PMID:16483794.
 [31] Lin JS, Lai EM. Protein-Protein Interactions: Co-Immunoprecipitation. Methods Mol Biol 2017;1615:211–219. doi:10.1007/978-1-4939-7033-2017.2018.2017.2017. 9_17, PMID:28667615. [32] Livak KJ, Schmittgen TD. Analysis of relative gene expression data using
- real-time quantitative PCR and the 2(-Delta Delta C(T)) Method. Methods 2001;25(4):402–408. doi:10.1006/meth.2001.1262, PMID:11846609. [33] Harms PW, Frankel TL, Moutafi M, Rao A, Rimm DL, Taube JM, et al. Multi-
- plex Immunohistochemistry and Immunofluorescence: A Practical Update for Pathologists. Mod Pathol 2023;36(7):100197. doi:10.1016/j.mod-pat.2023.100197, PMID:37105494.
- [34] McCarty KS Jr, Szabo E, Flowers JL, Cox EB, Leight GS, Miller L, et al. Use of a monoclonal anti-estrogen receptor antibody in the immunohistochemical evaluation of human tumors. Cancer Res 1986;46(8 Suppl):4244s-4248s. PMID:3524805.
- [35] Franken NA, Rodermond HM, Stap J, Haveman J, van Bree C. Clonogenic assay of cells in vitro. Nat Protoc 2006;1(5):2315–2319. doi:10.1038/ nprot.2006.339, PMID:17406473.
- [36] Salic A, Mitchison TJ. A chemical method for fast and sensitive detection of DNA synthesis in vivo. Proc Natl Acad Sci U S A 2008;105(7):2415–2420. doi:10.1073/pnas.0712168105, PMID:18272492.
- doi:10.1073/pnas.0712168105, PMID:18272492.
 [37] Liang CC, Park AY, Guan JL. In vitro scratch assay: a convenient and inexpensive method for analysis of cell migration in vitro. Nat Protoc 2007;2(2):329–333. doi:10.1038/nprot.2007.30, PMID:17406593.
 [38] Kleinman HK, Martin GR. Matrigel: basement membrane matrix with biological activity. Semin Cancer Biol 2005;15(5):378–386. doi:10.1016/j. semcancer.2005.05.004, PMID:15975825.
 [39] Takahashi Y, Fukusato T. Histopathology of nonalcoholic fatty liver disease/nonalcoholic steatohepatitis. World J Gastroenterol 2014;20(42):15539–15548. doi:10.3748/wig.v20.i42.15539, PMID:25400438.
 [40] Balduyck L, Veryser C, Goiris K, Bruneel C, Muylaert K, Foubert I. Optimization of a Nile Red method for rapid lipid determination in autotrophic, marine microalgae is species dependent. J Microbiol Methods 2015:118:152-

- rine microalgae is species dependent. J Microbiol Methods 2015;118:152–158. doi:10.1016/j.mimet.2015.09.009, PMID:26388510.
- [41] Fossati P, Prencipe L. Serum triglycerides determined colorimetrically with an enzyme that produces hydrogen peroxide. Clin Chem 1982;28(10):2077–2080. PMID:6812986.
 [42] Allain CC, Poon LS, Chan CS, Richmond W, Fu PC. Enzymatic determination of total serum cholesterol. Clin Chem 1974;20(4):470–475. PMID: 4919200.
- 4818200.
- [43] Christmass MA, Mitoulas LR, Hartmann PE, Arthur PG. A semiautomated enzymatic method for determination of nonesterified fatty acid concentration in milk and plasma. Lipids 1998;33(10):1043-1049. doi:10.1007/
- s11745-998-0304-9, PMID:9832086.
 [44] Kratka K, Sistik P, Olivkova I, Kusnierova P, Svagera Z, Stejskal D. Mass Spectrometry-Based Proteomics in Clinical Diagnosis of Amyloidosis and Multiple Myeloma: A Review (2012-2024). J Mass Spectrom
- 2025;60(3):e5116. doi:10.1002/jms.5116, PMID:39967472.

 [45] Zhou C, Weng J, Liu C, Liu S, Hu Z, Xie X, *et al.* Disruption of SLFN11 Deficiency-Induced CCL2 Signaling and Macrophage M2 Polarization Potentiates Anti-PD-1 Therapy Efficacy in Hepatocellular Carcinoma. Gastro-

- enterology 2023;164(7):1261-1278. doi:10.1053/j.gastro.2023.02.005,
- PMID: 36863689. [46] Ogasawara S, Mihara Y, Kondo R, Kusano H, Akiba J, Yano H. Antiprolifera-
- [46] Ogasawara S, Mihara Y, Kondo R, Kusano H, Akiba J, Yano H. Antiproliferative Effect of Lenvatinib on Human Liver Cancer Cell Lines In Vitro and In Vivo. Anticancer Res 2019;39(11):5973–5982. doi:10.21873/anticanres.13802, PMID:31704822.
 [47] Wang Y, Zhao Z, Guo T, Wu T, Zhang M, Luo D, et al. SOCS5-RBMX stimulates SREBP1-mediated lipogenesis to promote metastasis in steatotic HCC with HBV-related cirrhosis. NPJ Precis Oncol 2024;8(1):58. doi:10.1038/s41698-024-00545-6, PMID:38429411.
 [48] Chen Y, Yong H, Chen M, Dang C, Wang P, Chu S, et al. TRIM21 attenuates.
- [48] Chen X, Yong H, Chen M, Deng C, Wang P, Chu S, et al. TRIM21 attenuates renal carcinoma lipogenesis and malignancy by regulating SREBF1 protein stability. J Exp Clin Cancer Res 2023;42(1):34. doi:10.1186/s13046-022-02583-z, PMID:36694250.
- 02583-z, PMID:36694250.
 [49] Han J, Li E, Chen L, Zhang Y, Wei F, Liu J, et al. The CREB coactivator CRTC2 controls hepatic lipid metabolism by regulating SREBP1. Nature 2015;524(7564):243-246. doi:10.1038/nature14557, PMID:26147081.
 [50] Cheng C, Ru P, Geng F, Liu J, Yoo JY, Wu X, et al. Glucose-Mediated N-glycosylation of SCAP Is Essential for SREBP-1 Activation and Tumor Growth. Cancer Cell 2015;28(5):569-581. doi:10.1016/j.ccell.2015.09.021, PMID:26555173.
 [51] Weng C, Tong Y, Weng Y, Cai J, Cup H, Hunge L, et al. Hepatocellular Cap.
- [51] Wang C, Tong Y, Wen Y, Cai J, Guo H, Huang L, et al. Hepatocellular Carcinoma-Associated Protein TD26 Interacts and Enhances Sterol Regula-

- tory Element-Binding Protein 1 Activity to Promote Tumor Cell Proliferation and Growth. Hepatology 2018;68(5):1833–1850. doi:10.1002/hep.30030, PMID:29663480.
- [52] Chan LL, Chan SL. The evolving role of lenvatinib at the new era of first-line
- hepatocellular carcinoma treatment. Clin Mol Hepatol 2023;29(4):909–923. doi:10.3350/cmh.2023.0114, PMID:37226446.

 [53] Mok EHK, Leung CON, Zhou L, Lei MML, Leung HW, Tong M, et al. Caspase-3-Induced Activation of SREBP2 Drives Drug Resistance via Promotion of Cholesterol Biosynthesis in Hepatocellular Carcinoma. Cancer Res 2022;82(17):3102–3115. doi:10.1158/0008-5472.CAN-21-2934, PMID:35767704 PMID:35767704. [54] Liu Y, Sun L, Guo H, Zhou S, Wang C, Ji C, et al. Targeting SLP2-mediat-
- ed lipid metabolism reprograming restricts proliferation and metastasis of hepatocellular carcinoma and promotes sensitivity to Lenvatinib. Oncogene
- 2023;42(5):374–388. doi:10.1038/s41388-022-02551-z, PMID:36473908.

 [55] Daum AK, Schlicker L, Schneider MA, Muley T, Klingmüller U, Schulze A, et al. Cancer-associated fibroblasts promote drug resistance in ALK-driven lung adenocarcinoma cells by upregulating lipid biosynthesis. Cancer Metab 2025;13(1):28. doi:10.1186/s40170-025-00400-7, PMID:40524253.
- [56] Kuang B, Geng N, Yi M, Zeng Q, Fan M, Xian M, et al. Panaxatriol exerts anti-senescence effects and alleviates osteoarthritis and cartilage repair fibrosis by targeting UFL1. J Adv Res 2025;74:493-511. doi:10.1016/j. jare.2024.10.016, PMID:39442872.